ELSEVIER

Polymer 42 (2001) 4281–4288

polymer

www.elsevier.nl/locate/polymer

Influence of a block copolymer on flow-induced phase-inverted morphology of an immiscible blend

J.R. Kim, S.D. Hudson, A.M. Jamieson*, I. Manas-Zloczower, H. Ishida

Department of Macromolecular Science, Case Western Reserve University, 2100 Adelbert Road, Cleveland, OH 44106-7202, USA

Received 5 July 2000; received in revised form 11 September 2000; accepted 13 September 2000

Abstract

The flow-induced morphology of ternary blends containing poly(styrene-*co*-acrylonitrile) (SAN) random copolymer as major phase, polystyrene (PS) as minor phase, and poly(styrene-*b*-methylmethacrylate) (PS-*b*-PMMA) block copolymer as emulsifier is investigated as a function of the acrylonitrile content of the SAN copolymer. In this way, the degree of exothermic interaction and swelling power between SAN and PMMA block is varied systematically. Consistent with previous work, a well-emulsified morphology is produced when the swelling tendency of the block segment in the major phase (S_{out}) is comparable to that in the minor phase (S_{int}) ($0.4 \leq S_{out}/S_{int} \leq 2.5$). Outside this window, emulsification failure occurs. We further investigate the influence of S_{out}/S_{int} on the formation of phase-inverted (PIN) morphology, induced by lowering the viscosity of the disperse phase. We demonstrate that a decrease in swelling power assists the tendency of the minor phase to be continuous, i.e. the formation of PIN structure is possible at a lower weight fraction of the minor component.

Keywords: Block copolymer; Phase-inverted morphology; Swelling power

1. Introduction

A finely-divided dispersion of the minor phase in an immiscible polymer blend is crucial for the optimal material properties of the blend. Two types of morphology have practical significance: (a) the situation where the minor phase is dispersed in the form of discrete droplets; and (b) phase-inverted (PIN) morphology, where the minor phase is induced to become the continuous phase. The former situation has been well-studied. Droplet radius (R) in a blend subjected to a shear field is governed [1] by the balance between the applied shear stress ($\eta_m\dot{\gamma}$) and the interfacial stress (Γ/R), defined by the capillary number, Ca:

$$\mathrm{Ca} = \frac{\eta_m\dot{\gamma}}{\Gamma/R} = \frac{\eta_m\dot{\gamma}R}{\Gamma}, \tag{1}$$

where Γ is the interfacial tension, $\dot{\gamma}$ the shear rate, and η_m the viscosity of the matrix. When Ca is larger than a critical value $\mathrm{Ca_c}$, the droplet is unstable and will break up under shear into smaller droplets; when Ca is less than $\mathrm{Ca_c}$, the droplet is stable in the shear field. $\mathrm{Ca_c}$ depends on the viscosity ratio $\eta_r = \eta_d/\eta_m$, where η_d is the droplet viscosity: when $\eta_r = 1$, $\mathrm{Ca_c}$ exhibits a minimum value at $\mathrm{Ca_c} \approx 0.5$; when, $\eta_r > 4$, droplet breakup does not occur since the droplet does not deform but instead exhibits rotational motion in the shear field. The following empirical equation has been proposed, based on Grace's experimental data for mixtures of Newtonian fluids in a laminar flow field [2,3]:

$$\log(\mathrm{Ca_c}) = -0.506 - 0.0994\log\eta_r + 0.124\log^2\eta_r - \frac{0.115}{\log\eta_r - \log\eta_{r,cr}}, \tag{2}$$

where $\eta_{r,cr} = 4.08$ is the critical relative viscosity above which droplet breakup is no longer possible in shear flow. In typical polymer blends, droplet sizes observed are often much larger than predicted by Eq. (2). This is generally attributed to the fact that, in shear flow, droplets can coalesce into larger droplets [4]. In some cases, the elasticity of the blend components [5] may also contribute, in part, to an increase in droplet size. The tendency to form PIN morphology during mixing in the melt state is enhanced by lowering the viscosity of the disperse phase. Specifically, it is reported that, for binary blends, the volume fraction of the minor component where phase inversion occurs depends on the viscosity ratio between

* Corresponding author. Tel.: +1-216-368-4172; fax: +1-216-368-4202.
E-mail address: macro@po.cwru.edu (A.M. Jamieson).

0032-3861/01/$ - see front matter
PII: S0032-3861(00)00753-9

Table 1
Acronyms and average molecular weights of polymers samples

Name	Acronym	M_n (kDa)	M_w (kDa)	M_w/M_n
PS-*b*-PMMA diblock copolymer[a]	BCP	143.8/154.8	160.5/173.4	1.12
Polystyrene[b]	PS50k	47.2	50	1.06
	PS18k	16.8	17.5	1.04
Styrene acrylonitrile copolymer[c] (26% AN content)	SAN26	68.6	153.0	2.23
Styrene acrylonitrile copolymer[c] (29% AN content)	SAN29	68.3	151.0	2.21
Styrene acrylonitrile copolymer[c] (33% AN content)	SAN33	66.7	130.1	1.95

[a] Purchased from Polymer Source Inc.
[b] Purchased from Pressure Chemicals.
[c] Supplied by Mitsui Toatsu Chemicals Inc.

the major and the minor phase [6]

$$\frac{\phi_{\text{major}}}{\phi_{\text{minor}}}\frac{\eta_{\text{minor}}}{\eta_{\text{major}}} \approx 1. \tag{3}$$

Block copolymers (BCPs) are known to function as emulsifiers for immiscible blends. It is generally accepted that emulsification occurs because the reduction of interfacial tension produces smaller droplets during breakup by decreasing the interfacial stress, as is evident from Eq. (1). In addition, recent evidence indicates that the BCP has an even more important role as an inhibitor for droplet coalescence [4,7–12]. The presence of BCP at the interface between droplet and matrix can suppress droplet coalescence by rendering the interface more rigid, and hence increasing the hydrodynamic interaction between droplets during collisions and/or inhibiting the drainage of the matrix between droplets during collisions [12].

Recently, we have investigated the role played by the thermodynamic interactions between a BCP and the blend components [9–11,13–15]. Interpretation of these data is most conveniently framed in terms of the spontaneous curvature of the interface in the presence of BCP [16]. An asymmetry ratio (σ_r) can be defined for long-chain BCP in a shorter-chain polymeric solvent [11,17]:

$$\sigma_r = [N_A S_A]/[N_B S_B], \tag{4}$$

where N_i are the degrees of polymerization of the BCP segments and S_i are the corresponding segmental swelling factors, given by the expression:

$$S_i = \left(\frac{N_i}{P} - N_i\chi\right), \tag{5}$$

where P is the degree of polymerization of the solvent compatible with block i, and χ is the relevant Flory–Huggins parameter. A value $\sigma_r = 1$ corresponds to zero spontaneous curvature.

In studies of solvent-cast blends, Adeyinka et al. [13] and Adedeji et al. [14,15] observed emulsification failure, an effect well known in emulsions of low molecular weight materials [18], when the swelling power of the segment in contact with the major phase (S_{out}) is much larger than that of the segment in contact with the minor phase (S_{int}). As is evident from Eq. (5), this effect can be produced by arranging a sufficiently large ratio *N/P* or a strong exothermic interaction. Conversely, Adeyinka et al. [13] and Adedeji et al. [14,15] showed that it is possible to lower dramatically the volume fraction of the minor phase at which PIN morphology is observed, if S_{int} is much stronger than S_{out}.

Kim et al. subsequently extended these studies to ternary blends mixed in the melt state [9–11]. The RMS 800 rheometer with parallel plate geometry was used as a mixing tool to avoid the complex deformation fields in a conventional mixer. Again, evidence was obtained that the balance between S_{out} and S_{int} at the interface between droplet and matrix is important in determining the flow-induced blend morphology. Too large an imbalance leads to the development of a coarse morphology because of either external ($S_{out} \gg S_{int}$) or internal ($S_{out} \ll S_{int}$) emulsification failure [9–11]. Thus, effective emulsification occurs in a window defined approximately by the boundaries

$$0.4 \leq S_{out}/S_{int} \leq 2.5. \tag{6}$$

In this study, we investigate the flow-induced morphology of blends consisting of poly(styrene-*co*-acrylonitrile) (SAN) random copolymer and polystyrene (PS), as major and minor components, respectively, with poly(styrene-*b*-methylmethacrylate) (PS-*b*-PMMA) diblock copolymer as emulsifier. By increasing the AN content of the SAN*x* copolymer between $x = 26\%$ AN and $x = 33\%$ AN, and keeping molecular weight constant, the exothermic interaction χ between the PMMA BCP segment and SAN*x* is decreased [19]. This means that the influence of a change in the swelling power S_i on flow-induced morphology can be explored in the compatibilized blend system without significantly changing the viscosities of the components. Our particular focus is on the change in morphology, which occurs when we decrease the viscosity of the minor component, and hence encourages the formation of PIN morphology. We further investigate the influence of the BCP segmental swelling power on the tendency for phase inversion.

2. Experimental

2.1. Materials

The molecular weights and polydispersities of the materials used are presented in Table 1 with their acronyms. In this study, droplet breakup and coalescence in SAN26/PS,

Table 2
Calculated values of polymer viscosities, Flory–Huggins parameter (χ), interfacial tension (Γ), and weight average droplet size (D)

	SAN26/PS50k		SAN33/PS50k	
$\dot{\gamma}$ (s^{-1})	20	1	20	1
η_m (Pa s)	2080	7210	1920	6130
η_d (Pa s)	57	82	57	82
η_r	0.027	0.011	0.03	0.013
χ	0.048		>0.078	
Γ (mN/m)	2.5		3.1	
D_{Grace} (μm)	0.06	1.18	0.08	1.72
$D_{Experiment}$ (μm)	1.1	2.5	1.5	3.1

SAN29/PS, and SAN33/PS blends containing a symmetric PS-*b*-PMMA BCP are investigated. SAN has exothermic interaction with PMMA when the AN content of the SAN copolymer is in the range between 15 and 33%. The degree of exothermic interaction increases with the decrease of the AN content of SAN. In this study, SAN containing 26, 29, and 33% of AN are utilized.

2.2. Sample preparation

In preparing polymer blends by solvent casting, solutions of SAN, PS and BCP were made up in MEK solvent at a concentration of 1 g/100 ml. Solutions containing SAN, PS and BCP in appropriate amounts were made by mixing stock solutions. The ratio of SAN to PS was fixed at 8:2 and 5% of BCP was added to the blend system without changing that ratio. The solvent was slowly evaporated from the ternary solutions over 14 days at room temperature, and the final solvent traces were removed by drying at 70°C for 24 h at atmospheric pressure, and drying under vacuum for another 24 h.

For melt blending in the rheometer, crude mixtures were first prepared by dry mixing the blend components in powder form. In preparing blends containing the BCP, the BCP and the minor phase constituent PS were first dissolved in MEK solvent, co-precipitated by adding methanol, a nonsolvent for all three polymeric segments, and the precipitates were dried in vacuum oven for 24 h at room temperature. This material in powder form was then dry mixed with the major phase. This procedure facilitates the migration of the BCP to the phase boundary [9–11]. The dry mixed powders were molded to form disks at 200°C under vacuum in a Carver Lab Press compression molding machine.

2.3. Viscosity measurement

Shear viscosities were measured as a function of shear rate at 200°C for SAN26, SAN33, and PS using the RMS 800 rheometer with parallel plate geometry. Viscosity values at 1 and 50 s^{-1} are listed in Table 2.

2.4. Processing

Disk samples, prepared as described above, were sheared in parallel plate geometry with diameter 7.9 mm and gap 0.5 mm at 200°C, using the RMS 800 rheometer. Shearing was first performed at a higher shear rate of 50 s^{-1} to produce breakup of large droplets of the minor phase. After shearing at a high shear rate for 20 min, a low shear

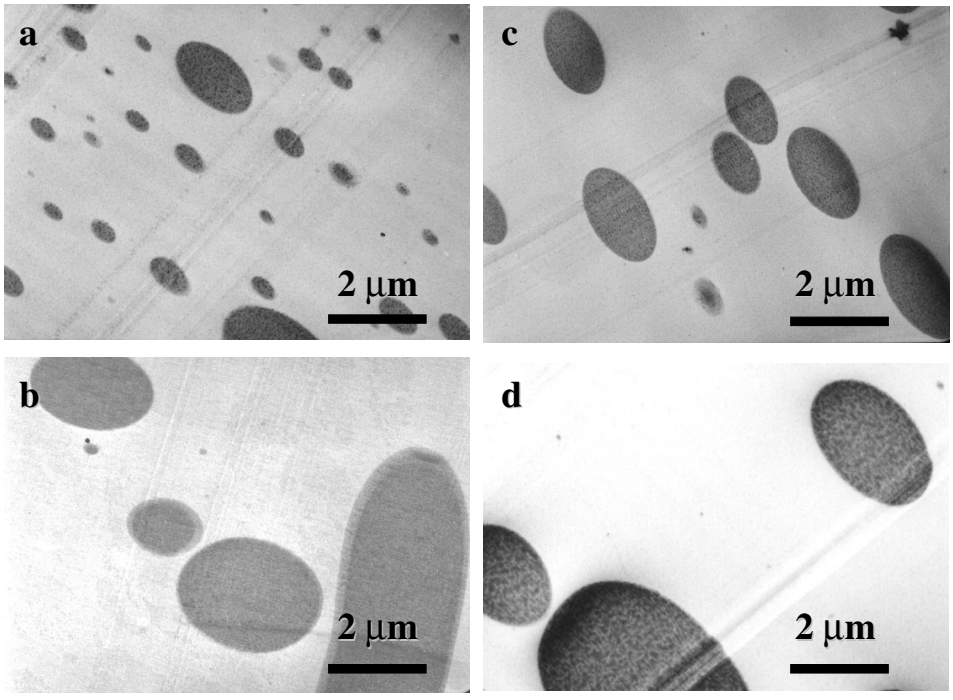

Fig. 1. TEM micrographs of binary blends: (a) SAN26/PS50 sheared at 20 s^{-1} for 20 min; (b) SAN26/PS50 sheared at 1 s^{-1} for 10 min following pre-shear at 20 s^{-1} for 20 min; (c) SAN33/PS50 sheared at 20 s^{-1} for 20 min; and (d) SAN33/PS50 sheared at 1 s^{-1} for 10 min following pre-shear at 20 s^{-1} for 20 min.

Table 3
Swelling powers of BCP segments in ternary blends

	S_{out}	S_{int}	(S_{out}/S_{int})
SAN26/PS50k/BCP	61.6	6.1	10.1
SAN29/PS50k/BCP	43.4	6.1	7.1
SAN33/PS50k/BCP	7.0	6.1	1.1
SAN26/PS18k/BCP	61.6	17.2	3.6
SAN33/PS18k/BCP	7.0	17.2	0.41

rate of 1 s^{-1} was applied consecutively and continued for another 20 min to allow shear-induced coalescence of the small droplets. After 1 min of equilibration, the samples were thermally quenched with liquid nitrogen. The time for the temperature to fall from the processing condition at 200°C to the glass transition (~100°C) was approximately 30 s.

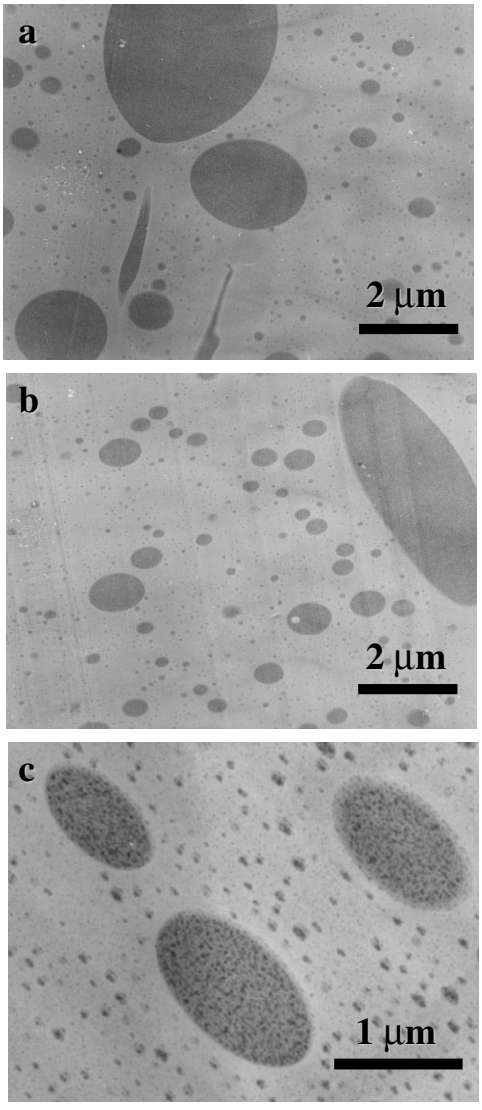

Fig. 2. TEM micrographs of ternary blends: (a) SAN26/PS50/BCP sheared at 20 s^{-1} for 20 min; (b) SAN26/PS50/BCP sheared at 1 s^{-1} for 20 min following pre-shear at 20 s^{-1} for 20 min; and (c) SAN33/PS50/BCP cast from solution.

2.5. Analysis

A JEOL 100 CX TEM with an acceleration voltage of 100 kV was used to investigate the morphologies of blends prepared both by melt blending and solvent casting. For the TEM observation to investigate the maximum shear region of the sample, the perimeter edge areas of the melt blended disk specimens were sectioned into ultrathin films of 50–80 nm thickness using a diamond knife and an RMC Inc. MT-7000 ultramicrotome machine. Sectioned films were exposed to RuO_4 vapor for 14 min in an enclosed chamber containing 0.25% aqueous solution of RuO_4. The PS blend component and the PS segment of the BCP, as well as the SANs are stained with RuO_4 such that the PS segment is seen as the darkest image, and the SAN major phase is light gray.

2.6. Image analysis

NIH image software [20] was used to calculate the statistical sizes of the droplets from the TEM micrographs of the blends. Weight average droplet diameters were calculated. The number of droplets calculated was at least 100 except in the case of 20 min of shearing time at 1 s^{-1} for the systems without BCP, in which at least 5–10 droplets were used to calculate the average droplet sizes due to a too large droplet size. The accuracy of binary thresholded images was checked, by comparing with the original images. For non-spherical droplets, diameters were obtained from the areas of ellipsoidal droplets using the equation, Area $= \pi(D/2)^2$, where the areas of the droplets were determined by the NIH software.

3. Results and discussion

3.1. Uncompatibilized blends

TEM micrographs for uncompatibilized blends SAN26/PS50k and SAN33/PS50k are shown in Fig. 1. The droplet size for SAN26/PS50k after breakup at high shear (20 s^{-1}) for 20 min (Fig. 1(a)) is smaller than that for SAN33/PS50k (Fig. 1(c)). This is consistent with the expectation that, in view of its higher χ value (Table 2), SAN33/PS50k has a higher interfacial tension compared to SAN26/PS50k. Both blends show coalescence 10 min after subsequent step-down to low shear rate (1 s^{-1}) (Fig. 1(b) and (d)). The volume-average droplet sizes were estimated using the NIH image analysis software and are listed in Table 2, together with the droplet sizes calculated from Eq. (2). Since the viscosity ratios for the two blend systems are very small (Table 2), the droplet breakup process is not as efficient as for blends where η_r is close to unity. Table 2 indicates that the predicted droplet sizes are much smaller

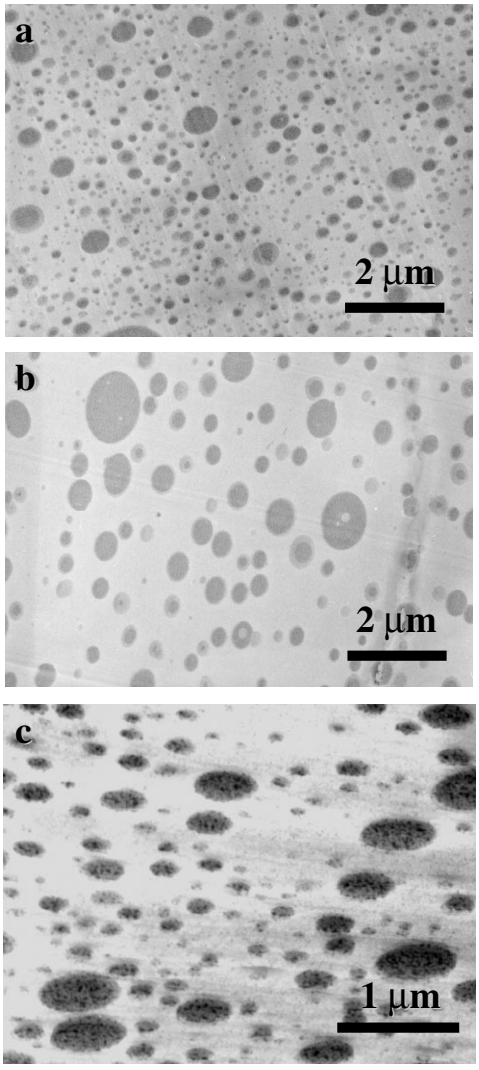

Fig. 3. TEM micrographs of ternary blends: (a) SAN33/PS50/BCP sheared at 20 s^{-1} for 20 min; (b) SAN33/PS50/BCP sheared at 1 s^{-1} for 20 min following pre-shear at 20 s^{-1} for 20 min; and (c) SAN26/PS50/BCP cast from solution.

than the experimental ones. A similar discrepancy was observed in our previous studies [9–11] on a different blend system. Potential sources of this inconsistency are [9–11] the coalescence of droplets due to the high concentration of the minor PS component (20 wt%) [4], and/or neglect of the non-Newtonian characteristics and elasticity of the blend components [5].

3.2. Compatibilized blends

Swelling powers for each BCP segment located at the droplet interface in the polymer blends studied were estimated using Eq. (2), and are listed in Table 3. TEM micrographs for SAN26/PS(50k)/BCP are shown in Fig. 2(a) and (b). Very small droplets coexist with large droplets both after shearing at high shear rate (20 s^{-1}) for 20 min (Fig. 2(a)), and after subsequent step-down to low shear (1 s^{-1}) for 20 min (Fig. 2(b)). This is a morphology typical of emulsification failure, and results from the large spontaneous interfacial curvature, due to the imbalance in the swelling power ratio ($S_{out}/S_{int} = 10.1$) between the external PMMA block (solubilized by SAN26) and the internal PS block (solubilized by PS homopolymer). In previous works [9–11], we have shown that, under these conditions, the coalescence of droplets is accompanied by migration of the BCP away from the interface to form micelles. One other contributing factor could be tip-streaming, which arises because an elongated droplet can have a variable local interfacial tension. This induces a sigmoidal shape of the droplet under a shear deformation, and the sharp tips of the sigmoidal droplets stream out very small droplets. Originally this mechanism was observed in uncompatiblized blends with low viscosity ratios by Grace [2], but later de Bruijn [21] argued that the tip streaming mechanism is possible only if there is surfactant in the system and hence that the observation by Grace appears to be due to impurities. We also examined the morphology of the SAN29/PS50k/BCP blend at high shear rate (20 s^{-1}) and following a step-down to low shear rate (1 s^{-1}). Again, we observed features typical of external emulsification failure both at high and at low shear rates. Evidently, the imbalance in BCP segmental swelling factor ($S_{out}/S_{int} = 7.1$) in this blend remains too large for effective emulsification.

In Fig. 3, we present the morphology of the SAN33/PS50k/BCP blend. After breakup for 20 min at high shear (20 s^{-1}), Fig. 3(a) indicates that the minor PS phase is finely distributed into small droplets in the SAN33 matrix, i.e. more effective emulsification is achieved relative to the SAN26 and SAN29 blends. Clearly, the BCP is effective in lowering interfacial tension and facilitating droplet breakup. After subsequently applying low shear rate (1 s^{-1}) for 10 min, the droplets coalesce (Fig. 3(b)), but at a rate slower than that of the uncompatibilized blend. Thus the droplet size after coalescence remains small, with a relatively narrow distribution, compared to the SAN26 or SAN29 blends. These observations are again consistent with our earlier studies of a different blend system [9–11]. When the swelling powers of external and internal blocks at the droplet interface are approximately balanced (here $S_{out}/S_{int} = 1.1$), the BCP is able to evenly distribute over the relatively flat interfaces of all of the droplets without conformational distortion. Thus the BCP does not induce emulsification failure and is effective in reducing the rate of coalescence.

The morphologies of solvent-cast SAN26 and SAN33, each blended with PS50k and PMMA-*b*-PS BCP, are shown in Figs. 2(c) and 3(c), respectively. The SAN26/PS50k/BCP blend, having the highest swelling power ratio ($S_{out}/S_{int} = 10.1$), exhibits characteristic emulsification failure (Fig. 2(c)), i.e. very small droplets (swollen micelles) and large minor phase domains coexist in the continuous phase. Emulsification failure is also observed in the SAN29/PS50k/BCP blend which, however, has a slightly smaller

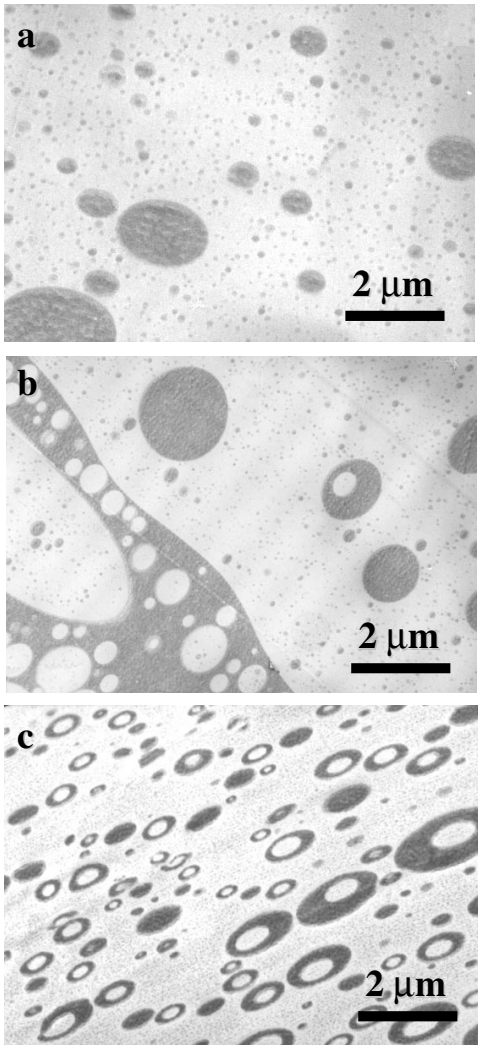

Fig. 4. TEM micrographs of ternary blends: (a) SAN26/PS18/BCP sheared at 50 s^{-1} for 20 min; (b) SAN26/PS18/BCP sheared at 1 s^{-1} for 20 min following pre-shear at 50 s^{-1} for 20 min; and (c) SAN26/PS18/BCP cast from solution.

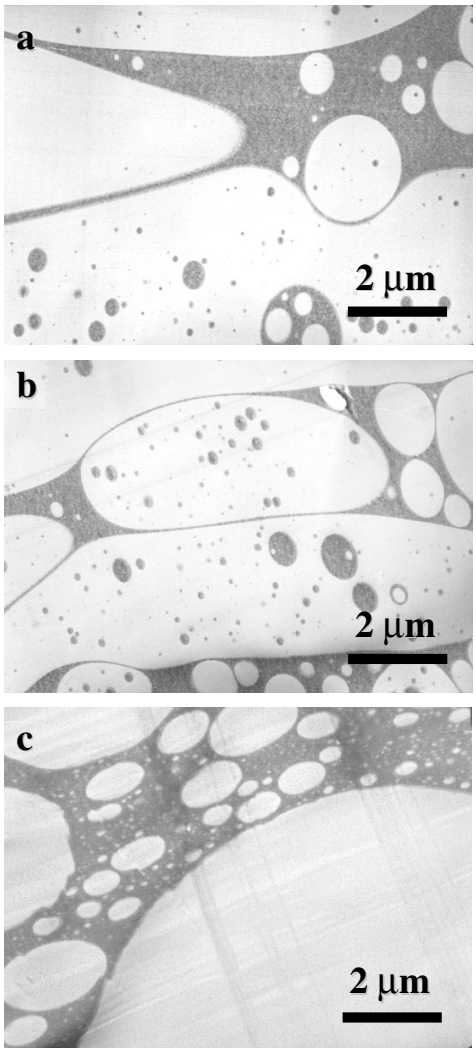

Fig. 5. TEM micrographs of ternary blends: (a) SAN33/PS18/BCP sheared at 50 s^{-1} for 20 min; (b) SAN33/PS18/BCP sheared at 1 s^{-1} for 20 min following pre-shear at 50 s^{-1} for 20 min; and (c) SAN33/PS18/BCP cast from solution.

swelling power ratio ($S_{out}/S_{int} = 7.1$), and therefore the size of the small micelles increases due to a smaller spontaneous curvature. In contrast, the morphology of the SAN33/PS50k/BCP blend (Fig. 3(c)) is quite different, exhibiting well-dispersed minor phase droplets, consistent with the more balanced swelling power ratio ($S_{out}/S_{int} = 1.1$). Comparing Fig. 2(c) and (b), and Fig. 3(c) and (b), we see that the solvent-cast blend morphologies are very similar to those from melt blending, indicative that the breakup and coalescence process leads to a quasi-equilibrium morphology.

These results reinforce an earlier conclusion [9–11], viz. if an added BCP has a very large external swelling power, relative to the internal swelling power, $S_{out} \gg S_{int}$, or vice versa, $S_{out} \ll S_{int}$, a coarse morphology results due to emulsification failure. Thus, effective emulsification occurs only in a window, which, for a symmetric BCP, may be expressed approximately by $0.4 \leq S_{out}/S_{int} \leq 2.5$. These boundaries are to be viewed as approximate. Leibler [22] has given theoretical arguments which conclude that in the dry brush limit ($S \sim 1$), emulsification failure occurs when $0.45 \leq S_{out}/S_{int} \leq 2.2$. Thus, for optimal emulsification of the blends, a balance of swelling between each block is more important than the strength of the swelling power.

3.3. SAN/PS18k/BCP blends

Following the above results, it is of interest to investigate the formation of PIN morphology, induced by lowering the viscosity ratio $\eta_{minor}/\eta_{major}$ (cf. Eq. (3)). This can be done by decreasing the molecular weight of the PS minor phase which, however, also increases the swelling power of the PS BCP segment, i.e. we increase S_{int}, and therefore decrease the swelling ratio S_{out}/S_{int} which, in principle, is a further driving force to form PIN morphology [13–15]. In Fig. 4(a) and (b), the blend morphology of SAN26/PS18k/

Table 4
Measured viscosity and viscosity ratio for SAN/PS18k blends

	SAN26/PS18k		SAN33/PS18k	
$\dot{\gamma}$ (s^{-1})	50	1	50	1
η_m (Pa s)	1420	7210	1340	6130
η_d (Pa s)	12	12	12	12
η_r	0.0084	0.0017	0.0090	0.0020

BCP is shown, after shearing at 50 s^{-1} for 20 min, and following a step-down to a lower shear rate at 1 s^{-1} for 10 min, respectively. For comparison, the morphology of the solvent-cast blend for the same system is shown in Fig. 4(c). Fig. 4(a) indicates that, despite the increase in S_{out}/S_{int}, the morphology at high shear rate remains typical of emulsification failure, consistent with the fact that there is still a large imbalance in swelling power ($S_{out}/S_{int} = 3.1$). Upon subsequent shearing at low shear rate (Fig. 5(b)), coalescence occurs accompanied by a distinctive change in the morphology, suggesting a tendency towards phase inversion where the minor phase becomes the continuous phase and the major phase becomes the discrete phase. The driving force for this change is presumably the increase in viscosity of the SAN major phase (Table 4).

In the SAN26/PS(18K)/BCP blend, because the viscosity ratio $\eta_r = \eta_{minor}/\eta_{major}$ at low shear rate is smaller than at high shear rate (Table 4), Eq. (3) indicates that the fraction of minor component at the phase inversion point should decrease at low shear rate, which is consistent with the experimental trend (cf. Fig. 4(a) versus Fig. 4(b)). However, in view of Fig. 4(a), it is evident that phase inversion occurs at a volume fraction considerably in excess of that predicted by Eq. (3). The reason for this is not clear, but it may originate in either the elasticity of the major phase or in an effect due to the presence of the BCP at the interface. For comparison, in Fig. 4(c), the morphology of the solvent-cast blend indicates that the minor phase exists as vesicles, consistent with the increase in swelling power (S_{int}) of the PS BCP segment [13–15].

For the SAN33/PS18k/BCP blend the morphology, after melt mixing at high shear rate (50 s^{-1}) and following a step-down to low shear (1 s^{-1}), exhibits in each case PIN morphology (Fig. 5(a) and (b)), even though the viscosity ratio is essentially the same as that of the SAN26/PS18k/BCP blend (Table 2). Thus, we deduce that this difference arises from the change in the χ parameter, which results in a lower swelling ratio S_{out}/S_{int} for the SAN33/PS18k/BCP system (Table 3). In solvent-cast blends, Adedeji et al. [14,15] reported that the phase-inverted morphology is facilitated by a higher swelling power of the block having interaction with the minor phase. This is supported by the micrograph in Fig. 5(c) which demonstrates that the solvent-cast SAN33/PS18k/BCP blend indeed shows PIN morphology. Thus, by decreasing the molecular weight of the PS minor phase, we have increased S_{int} and demonstrated that a decrease in S_{out}/S_{int} below unity (Table 3) favors phase inversion in both flowing and quiescent conditions. Thus, both hydrodynamic and thermodynamic factors can be manipulated to cause the formation of PIN morphology at low volume fractions of the disperse phase.

4. Conclusions

The balance of swelling power between the outside and inside segments of the BCP at the interface of an immiscible blend is an important design factor for proper compatibilization. A severe imbalance in swelling power tends to produce emulsification failure. Even in the case of a severe viscosity imbalance ($\eta_r \sim 0.01$), when the BCP segments have a balance of swelling power at the interface ($S_{out}/S_{int} \sim 1$, e.g. in the SAN33/PS50k/BCP system), the blends are well emulsified at high shear and exhibit slow coalescence at low shear rate. When the viscosity ratio is reduced even further ($\eta_r \sim 0.02$), the flow-induced morphology tends towards phase-inverted structures, i.e. the lower viscosity PS minor phase becomes the continuous phase, and the major SAN phase is entrapped inside the PS phase. From our observation that the SAN33/PS18k/BCP blend more easily forms a phase-inverted structure, we conclude that, in addition to a small viscosity ratio, a decrease in the swelling power ratio S_{out}/S_{int} below unity favors phase inversion.

Acknowledgements

The financial support from the Edison Polymer Innovation Corporation, the General Electric Company, and NSF Grant CTS-9731502 is gratefully acknowledged.

References

[1] Taylor GI. Proc R Soc, London 1934;A146:501.
[2] Grace HP. Chem Engng Commun 1982;14:225.
[3] Minale M, Mewis J, Moldenaers P. AIChE J 1998;44:943.
[4] Sundararaj U, Macosko CW. Macromolecules 1995;28:2647.
[5] Mighri F, Carreau PJ, Ajji A. J Rheol 1998;42:1447.
[6] Jordhamo GM, Manson JA, Sperling LH. Polym Engng Sci 1986;26:517.
[7] Milner ST, Xi H. J Rheol 1996;40:663.
[8] Beck Tan NC, Tai S-K, Briber RM. Polymer 1996;37:3509.
[9] Kim JR, Jamieson AM, Hudson SD, Manas-Zloczower I, Ishida H. Macromolecules 1998;31:5383.
[10] Kim JR, Jamieson AM, Hudson SD, Manas-Zloczower I, Ishida H. Macromolecules 1999;32:4582.
[11] Kim JR, Hudson SD, Jamieson AM, Manas-Zloczower I, Ishida H. Polymer 2000;41:9163.
[12] Ramic AJ, Stehlin JC, Hudson SD, Jamieson AM, Manas-Zloczower I. Macromolecules 2000;33:371.
[13] Adedeji A, Hudson SD, Jamieson AM. Polymer 1997;38:737.
[14] Adedeji A, Jamieson AM, Hudson SD. Macromolecules 1995;28:5255.
[15] Adedeji A, Jamieson AM, Hudson SD. Macromol Chem Phys 1996;197:2521.

[16] Wang ZG, Safran SA. J Chem Phys 1991;94:679.
[17] Wang ZG. Private communication, 2000.
[18] Wang ZG, Safran SA. J Phys (France) 1990;51:185.
[19] Fowler ME, Barlow JW, Paul DR. Polymer 1987;28:2145.
[20] NIH Image Analysis Software. Available on the internet at http://rsb.info.nih.gov/nih-image/.
[21] de Bruijn RA. Chem Engng Sci 1993;48:277.
[22] Leibler L. Macromol Symp 1988;16:1.